

Physics-Inspired Deep Learning and Transferable Models for Bridge Scour Prediction

Negin Yousefpour, PhD, PE¹ and Bo Wang, PhD²

¹Department of Infrastructure Engineering, The University of Melbourne. Email: negin.yousefpour@unimelb.edu.au

²Department of Infrastructure Engineering, The University of Melbourne. Email: bo.wang@unimelb.edu.au

ABSTRACT

This paper introduces scour physics-inspired neural networks (SPINNs), a hybrid physics-data-driven framework for bridge scour prediction using deep learning. SPINNs integrate physics-based, empirical equations into deep neural networks and are trained using site-specific historical scour monitoring data. Long-short Term Memory Network (LSTM) and Convolutional Neural Network (CNN) are considered as the base deep learning (DL) models. We also explore transferable/general models, trained by aggregating datasets from a cluster of bridges, versus the site/bridge-specific models. Despite variation in performance, SPINNs outperformed pure data-driven models in the majority of cases. In some bridge cases, SPINN reduced forecasting errors by up to 50 percent. The pure data-driven models showed better transferability compared to hybrid models. The transferable DL models particularly proved effective for bridges with limited data. In addition, the calibrated time-dependent empirical equations derived from SPINNs showed great potential for maximum scour depth estimation, providing more accurate predictions compared to commonly used HEC-18 model. Comparing SPINNs with traditional empirical models indicates substantial improvements in scour prediction accuracy. This study can pave the way for further exploration of physics-inspired machine learning methods for scour prediction.

1 Introduction

Scour is recognized as the leading cause of bridge failure in many countries. In the United States, scour is responsible for approximately 60% of bridge failures ([Briaud J.L. et al., 2012](#)). Historical data from other countries and regions, such as Australia, Taiwan, Japan, Germany, France, and Iran, shows that a large

number of bridges have suffered scour-related failures due to typhoons and floods in the past few decades (Pizarro et al., 2020).

The complexity of predicting the expected maximum depth of scour at bridge piers stems from the intricate interactions between soil, hydrodynamic forces and the pier structure. Key challenges include uncertainties in riverbed material, flow conditions, geomorphological variations, and the increasing impacts of climate change. In recent decades, numerous research efforts have focused on developing empirical models to estimate scour depth using laboratory experiments and field observations. Despite these efforts, many empirical models tend to overestimate or underestimate scour depth due to their limited generalization across diverse riverbeds, flow, and structural conditions (Sheppard et al., 2011). For instance, the widely used HEC-18 scour equation, despite its evolution over the past two decades, has notable limitations, including insensitivity to various geological conditions, particularly to cohesive soils. Also, the empirical models are unable to provide a reliable assessment of scour variation with time and risk of scour failure, especially under flood conditions (Arneson et al., 2012). In response to this pressing need for more reliable predictive methods to enhance scour risk assessment and bridge safety, various Artificial Intelligence (AI) and Machine Learning (ML) methods have been explored. Readers are referred to Yousefpour et al. (2021), Yousefpour and Correa (2023), Hashem and Yousefpour (2024), and the cited references for a full literature review.

The ML models have been shown to outperform traditional empirical equations in estimating maximum scour depth. However, their performance remains restricted within the domain of training data and is highly dependent on the data quality and size, which are often scarce and do not cover a wide range of geological, hydraulic, and geomorphological conditions. In addition, these models are typically designed to predict the maximum scour depth for a given flow discharge and are not suitable for dynamic real-time forecasting. Given the limitations of current scour prediction models, bridge authorities have turned to monitoring solutions, including the use of continuous remote sensing systems enabling more reliable risk management for critical and large-scale bridges (NCHRP, 2009; Briaud et al., 2011). Pioneering works by Yousefpour et al. (2021), Yousefpour and Correa (2023), and Hashem and Yousefpour (2024) introduced deep learning (DL) solutions, specifically long-short-term memory (LSTM) networks and the convolutional neural network (CNN), for real-time scour forecasting. These models leverage LSTM and temporal CNN strength in temporal pattern recognition and capture the complex physical process of scour without direct feature extraction. By training on historical scour monitoring data, including time series of bed elevation, flow depth, and velocity, the DL models have shown the ability to predict upcoming scour depths up to a week in advance for case-study bridges in Alaska and Oregon.

Physics-based machine learning has accelerated as an emerging field in the past few years. The core idea is to incorporate physics law and constraints into the process of machine learning from data (Karpatne et al., 2017; Karniadakis et al., 2021). The hybrid physics-data-driven models have been introduced by a number of pioneering studies, referred to as physics-guided neural networks (PGNN) (Jia et al., 2021), physics-constrained neural networks (Raissi et al., 2019), and physics-informed neural networks (PINN) (Zhu et al., 2019). These terms have been used alternately in various recent studies (Faroughi et al., 2024). The incorporation of physical equations governing the input-response relationship, especially in the form of PDE/ODE within the loss function, is being increasingly referred to as physics-informed ML. PINNs have been particularly developed to solve PDEs in application to various problems in solid mechanics (Haghighat et al., 2021), porous media simulations (Chen et al., 2023; Amini et al., 2023), constitutive modelling, and soil consolidation (Eghbalian et al., 2023; Li et al., 2024a; Lan et al., 2024; Tian and Wang, 2023; Masi and Einav, 2024). Likewise PGNNs have found successful applications in structural analysis (Yu et al., 2020; Chen and Liu, 2021), geohazard assessment (Pei et al., 2023; Zhang et al., 2020) tunneling

(Li et al., 2024b), fluid mechanics (Yousif et al., 2022), among other fields.

This paper introduces hybrid physics-data-driven models for scour prediction. A novel physics-inspired deep learning framework is developed by integrating semi-empirical scour models with prominent deep learning algorithms. As closed-form equations are used in this study, and to avoid misinterpretations, the term "physics-inspired neural networks" is adopted. We introduce SPINNs, *Scour Physics-Inspired Neural Networks*, which leverage the temporal feature extraction capability of recurrent neural networks and convolutional neural networks, while respecting the physics driving the scour process.

The SPINNs are trained using historical scour monitoring data (more than 15 years) from a number of case-study bridges in Alaska. As a by-product of SPINNs, new empirical equations are introduced that are calibrated through deep learning algorithms. These DL-calibrated empirical equations can have superior performance over locally calibrated empirical models (e.g., HEC-18).

We also explore the viability of *transferable* scour models; these general models are trained with collective monitoring data from a cluster of bridges within a region and implemented to predict scour for individual bridges. The transferability of the proposed data-driven and hybrid models are investigated across the case studies and their accuracy is compared to bridge/site-specific models.

2 Approach

2.1 Notations and Definitions

To provide better clarity to our methodology, notations are provided in Table 1.

2.2 Scour Data and Preprocessing

The scour monitoring data of four bridges in Alaska is used to train the scour prediction models in this study. This data includes time series of the river bed, measured by sonar sensors at the bridge pier, and flow elevations, measured by stage sensors or gauges at the upstream, as well as river discharge, estimated based on measurement of flow velocity using velocimeter or Acoustic Doppler sensors. This data was provided by the Alaska Department of Transportation (DOT) and the US Geological Survey (USGS).

Some of the missing data, for example, the discharge data was obtained from the Alaska Science Center online platform¹. Most of the bridges on this platform contain the historical and real-time monitoring data collected from sonar and stage sensors attached to bridge piers with critical scour depth. The river discharge data in our methodology is only available for a few bridges at this point. Considering the data availability, we selected Bridge 212, 527, 539, and 742 with the key attributes presented in Table 2. The as-built bed elevation provides an important reference level to measure the scour depth. Pier and channel dimensions are listed in meters. Also, coefficients K_1 , K_2 , and K_3 are factors used in the HEC-18 empirical equations as defined in Table 1.

This paper mainly follows the same preprocessing method outlined in Yousefpour et al. (2021) and Yousefpour and Correa (2023) for the historical bridge scour monitoring dataset. The raw data is aggregated on an hourly basis. The key preprocessing steps include outlier removal, smoothing and denoising, and linear imputation of missing data. The data availability of each monitored attribute is impacted by many

¹<https://www.usgs.gov/centers/alaska-science-center/science/streambed-scour-bridges-alaska>

Table 1. Notations.

Symbol	Description	Unit
t	Timestep	<i>hour</i>
E_{stage}	Rive flow elevation measured by stage sensors at the upstream of the pier	<i>m</i>
E_{bed}	River bed elevation at the pier measured by Sonars	<i>m</i>
E_{ref}	Reference elevation for calculating local scour depth	<i>m</i>
y_s	Equilibrium scour depth	<i>m</i>
y_{st}	Time-dependent scour depth	<i>m</i>
y_1	Flow depth directly upstream of the pier	<i>m</i>
M_{in}	Input length (timesteps) of the NN	<i>N/A</i>
M_{out}	Output length (timesteps) of the NN	<i>N/A</i>
Y_s	Sequential forecasting targets contains observed scour depth values	<i>N/A</i>
\hat{Y}	The prediction on Y_s	<i>N/A</i>
\hat{Y}_{sNN}	The prediction on Y_s by NN model	<i>N/A</i>
\hat{Y}_{sPHY}	The prediction on Y_s by calibrated empirical equation	<i>N/A</i>
a	Pier width	<i>m</i>
L	Channel width	<i>m</i>
V	Mean velocity of flow directly upstream of the pier	<i>m/s</i>
g	Acceleration of gravity	$9.81m/s^2$
A	Cross-sectional area of flow	<i>m</i> ²
q	Average upstream discharge	<i>m</i> ³ / <i>s</i>
K_1	Correction factor for pier nose shape	<i>N/A</i>
K_2	Correction factor for angle of attack of flow	<i>N/A</i>
K_3	Correction factor for bed condition	<i>N/A</i>

factors, such as sensor reliability, seasonal river freezing, and flood occurrences. We synchronised E_{bed} , E_{stage} , and q , ensuring the timesteps used for training the models include these three input features.

Table 2. Attributes of Case-Study Bridges.

No	Name	As-built Bed- Elevation (m)	Channel Width (m)	Pier Width (m)	Pier Length (m)	Attack An- gle (°)	Pier Nose Shape	K_1	K_2	K_3
212	Kashwitna River	48.8	65.2	1.5	8.5	0	Sharp	0.9	1	1.1
527	Salcha River	193.2	153.3	1.2	10.7	10	Round	1	1.8	1.1
539	Knik River	10.4	152.7	1.3	7.9	0	Sharp	0.9	1	1.1
742	Chilkat River	35.2	152.4	1.5	7.3	0	Round	1	1	1.1

2.3 Physics-Inspired Deep Learning Framework

We introduce Scour Physics-inspired Neural Network (SPINN) as a new framework for scour prediction. This framework integrates an additional physical loss term using physics-based empirical equations. Over the past few decades, various semi-empirical equations have been developed to estimate local scour depth based on physical factors such as flow depth, flow velocity, pier geometry, and riverbed material/geology, calibrated based on laboratory and field testing (Sheppard et al., 2011; Arneson et al., 2012; Kirby et al., 2015). The overall architecture of SPINN is depicted in Fig. 1.

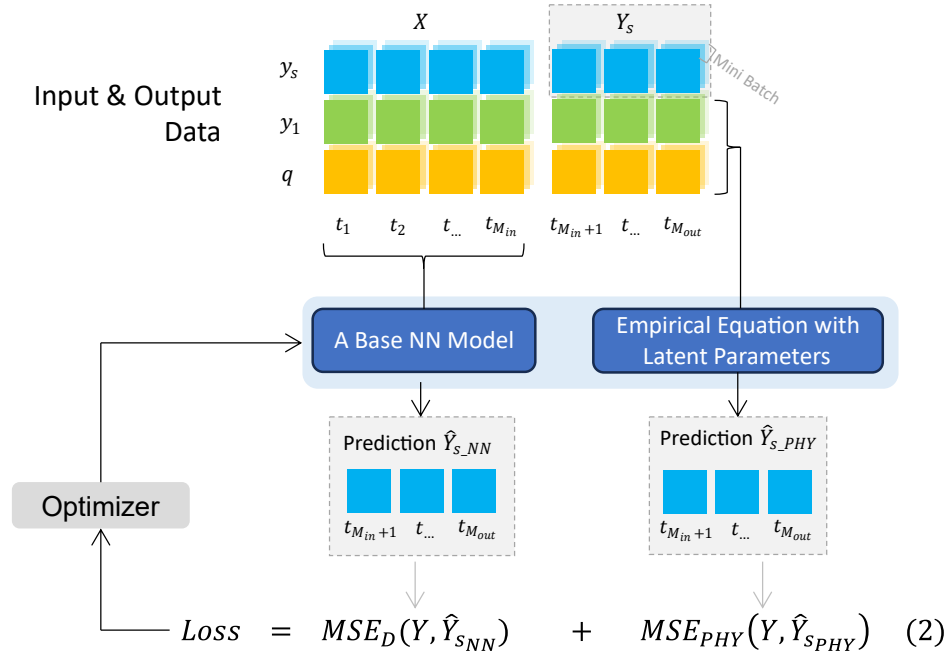


Fig. 1. SPINN framework, illustrating the integration of physics-based empirical equations as additional loss terms in the neural network training process.

The SPINN models are developed based on our pure data-driven LSTM and CNN scour forecast algorithms developed in Yousefpour and Correa (2023) and Hashem and Yousefpour (2024) for scour forecast based on historical sonar, stage, and discharge time series data. The SPINN model receives the time series data in a number of small slices each including an input part and output part. The input sequence X , includes scour depth, y_s , flow depth, y_1 , and discharge, q over M_{in} timesteps, while the output sequence, Y_s contains only scour depth, y_s over M_{out} timesteps. The discrepancy (loss) between the target (actual) scour depth (y_i) and the predicted scour depth (\hat{y}_i) is quantified over the output sequence, using the Mean Squared Error (MSE). As opposed to pure data-driven ML, the objective function is defined as the sum of two loss terms, a data-driven loss (MSE_D) and a physics-based loss (MSE_{PHY}), as described in Equations 1 and 2:

$$MSE = \sum_{i=0}^{M_{out}} (y_i - \hat{y}_i)^2 \quad (1)$$

$$Loss = MSE_D(Y, \hat{Y}_{s,NN}) + MSE_{PHY}(Y, \hat{Y}_{s,PHY}) \quad (2)$$

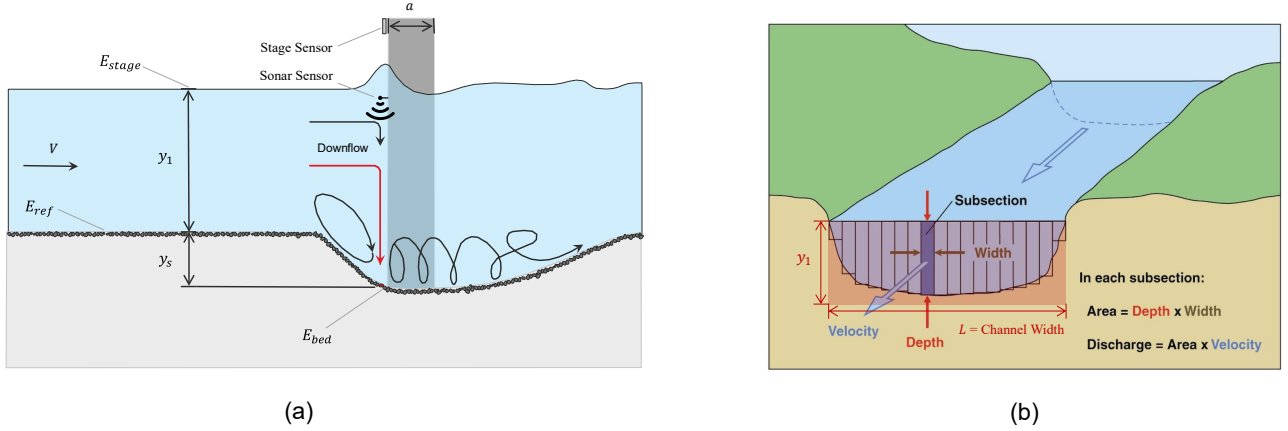


Fig. 2. a) Profile of pier subjected to scour, showing sensors and variables [adapted from Arneson et al. (2012)], b) Calculation of channel cross-sectional area and the relationship between velocity and discharge.

Within this framework, $\hat{Y}_{s_{NN}}$ represents the output from the base NN model (pure ML), and $\hat{Y}_{s_{PHY}}$ denotes the predictions yielded by the empirical equation (calibrated through ML training). For this purpose, the y_1 and q within the output timesteps (M_{out}) are used as input data for the physics empirical equation. By concurrently optimizing these two loss components, the SPINN model learns both from the inherent relationship within data and also satisfies the underlying governing physical relationship dictated by the empirical equation.

In this study, we implement three SPINN variants, with three empirical equations, including the widely accepted HEC-18 equation to a modified time-dependent form as described in the following sections. These equations involve latent parameters calibrated based on time series data throughout the training process. These parameters are optimized by Adam optimizer based on the total loss alongside the hidden parameters of the base NN model (Kingma and Ba, 2014).

2.3.1 SPINN with HEC18 Equation (SPINN-HEC18)

HEC-18, officially known as Hydraulic Engineering Circular No. 18, is a widely recognized engineering guideline published by the United States Federal Highway Administration (FHWA). This guideline provides recommendations for the prediction of maximum depth of scour. Over time, HEC-18 has undergone iterative revisions, with the most current version documented in Arneson et al. (2012). The latest HEC-18 Equation (3) is shown in Equation (3):

$$y_s = 2.0aK_1K_2K_3\left(\frac{y_1}{a}\right)^{0.35}\left(\frac{V}{gy_1^{0.5}}\right)^{0.65} \quad (3)$$

where y_s is the equilibrium scour depth, y_1 is the flow depth, a is the width of the pier, and K_1, K_2, K_3 , are correction factors related to the conditions of the pier, the flow and the riverbed as defined in Table 1. This equation is predominantly calibrated using datasets from laboratory measurements.

For training the SPINN model, we use time series of three features collected from continuous sensor measurements at bridge piers, including riverbed elevation, flow elevation and discharge, E_{bed} , E_{stage} , and q . Scour depth and flow depth, y_s and y_1 at each timestep can be derived by the following equations, as shown in Fig. 2a:

$$y_1 = E_{stage} - E_{ref} \quad (4)$$

$$y_s = E_{ref} - E_{bed} \quad (5)$$

where E_{stage} is the stage (elevation of the flow directly upstream of the pier), E_{bed} is the bed elevation, and E_{ref} is the reference level. For SPINN-HEC18, we use the as-built bed elevation as E_{ref} .

We derive average velocity (V) based on the time series of discharge data (q), as the direct measurements of velocity are not provided by USGS. As shown in Fig. 2b, discharge can be estimated by river channel cross-sectional area times velocity. The cross-sectional area of flow (A) is not easy to measure nor available in this study, therefore we assume that A can be calculated as $y_1 \times L$ multiplied by a fixed ratio $p_2 \in [0, 1]$, which can be estimated as a latent parameter within SPINN. Therefore, V can be calculated as:

$$V = \frac{q}{A} = \frac{q}{p_2 L y_1} \quad (6)$$

In addition, we include $p_1 \in [-1, 1]$ as another latent parameter that adjusts the combined correction factors (pier shape, flow direction, and riverbed). Therefore, the empirical equation, \hat{Y}_{sPHY} can be written as:

$$\hat{Y}_{sPHY} = p_1 2.0 K_1 K_2 K_3 \frac{a^{0.65}}{g^{0.215} L^{0.43} y_1^{0.295}} \left(\frac{q}{p_2} \right)^{0.43} \quad (7)$$

where p_1 and p_2 will be calibrated through the SPINN training process, resulting in a new calibrated empirical equation.

Equation 7 is only applicable during scouring episodes and not to filling episodes. To account for this, we impose a condition to include the physical loss term in the total loss only when y_s is greater than zero (i.e., $E_{ref} > E_{bed}$). When y_s becomes negative, which happens during filling episodes, the MSE_{PHY} term is set to zero for those specific mini-batches or sequences.

2.3.2 SPINN with Time-Dependent HEC18 Equation (SPINN-TD)

Our dataset records show that the Alaskan bridges experience live-bed scour, where the riverbed goes through iterative cycles of scouring and filling (Ngo, 2018). For each occurrence of a scour event, the progression of live-bed scour can be outlined into two distinct phases, as illustrated in Fig. 3a. In the initial growth phase, local scour begins from a depth of zero and gradually deepens. Upon reaching equilibrium depth, the local scour undergoes fluctuations, maintaining a relatively steady state. During this balanced phase, the flow dynamics lead to sediment deposition and erosion, resulting in a state of equilibrium. A number of time-dependent equations (Sheppard et al., 2011; Liang et al., 2019) have been developed to approximate the upper bound of scour depth, as depicted in Fig. 3b.

We define a time-dependent empirical model of scour based on the maximum scour depth ($y_{s,max}$) from HEC18 and an exponential decay function to account for time dependency as shown in Equation 8. In each data slice within a scour episode, the elevation at the first timestep is considered as E_{ref} , and the last timestep M_{out} within the target sequence is considered as the maximum scour depth.

$$\hat{y}_{st} = y_{s,max} \left(1 - e^{-\frac{p_3 \times t}{T_L}} \right) = p_1 2.0 K_1 K_2 K_3 \frac{a^{0.65}}{g^{0.215} L^{0.43} y_{1,max}^{0.295}} \left(\frac{q_{max}}{p_2} \right)^{0.43} \left(1 - e^{-\frac{p_3 \times t}{T_L}} \right) \quad (8)$$

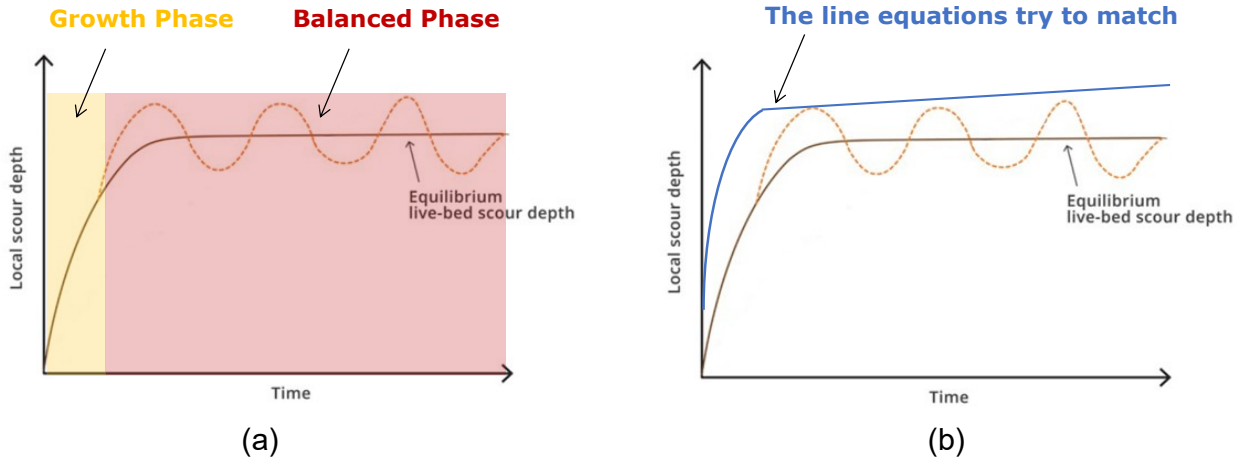


Fig. 3. Temporal features of live-bed local scour: a) Different phases of scour evolution, b) The ideal fitting line representing the upper bound of scour depth. Source: Ngo (2018).

In this equation, \hat{y}_{st} is the predicted time-dependent local scour depth at timestep t , where $t \in \{0, 1, 2, \dots, M_{out} - 1\}$ represents the time steps of the output sequence. T_L is the time lag between the maximum scour depth and the maximum flow, which is often observed in the scour process. This time lag is physically meaningful as it accounts for the delayed response of the scour depth to the flow conditions. p_1 , p_2 , and p_3 are latent parameters, where p_3 represents the decay rate in the exponential function, controlling how quickly the scour depth approaches the equilibrium state. These parameters are passed through a hyperbolic tangent (\tanh) activation function, which constrains their values to the range $[-1, 1]$. T_L is set to be within the range $[0, 2(M_{in} + M_{out})]$. By setting the upper limit of T_L to be twice the sum of M_{in} and M_{out} , we ensure that the parameter has sufficient flexibility to learn the appropriate time lag between the maximum scour depth and the maximum flow, even if the lag extends beyond the output sequence length.

Given that the time-dependent equation mentioned above is specifically applicable to instances of scouring episodes, it is important to identify these episodes as illustrated in Fig. 4. The training workflow for a single data batch comprises several key steps. Initially, the bed elevation values of the first timestep within the mini-batch are picked as the reference level E_{ref} for calculating flow depth and scour depth for each sequence, which are inputs for the NN model and the TD empirical equation. During this process, the sequences pass through the conditional term of physics loss (MSE_{PHY}) to filter scour episodes, similar to SPINN-HEC18 models. The physics loss is only applied to the scour episodes, therefore MSE_{PHY} term is set to zero for filling episodes/sequences.

Similar to SPINN-HEC18, the training is performed based on total loss for all mini-batches, including both scouring and filling episodes, to adjust the hidden parameters in the NN model and latent parameters in the TD empirical equation.

2.3.3 Transferable/General Time-Dependent Equation (SPINN-GTD)

Both SPINN-HEC18 and SPINN-TD are site/bridge-specific models and require abundance of site-specific data, including pier geometry, and correction factors for bed condition, and flow attack angle. In order to develop a general model that is transferable across multiple bridges within a region (a cluster of bridges with

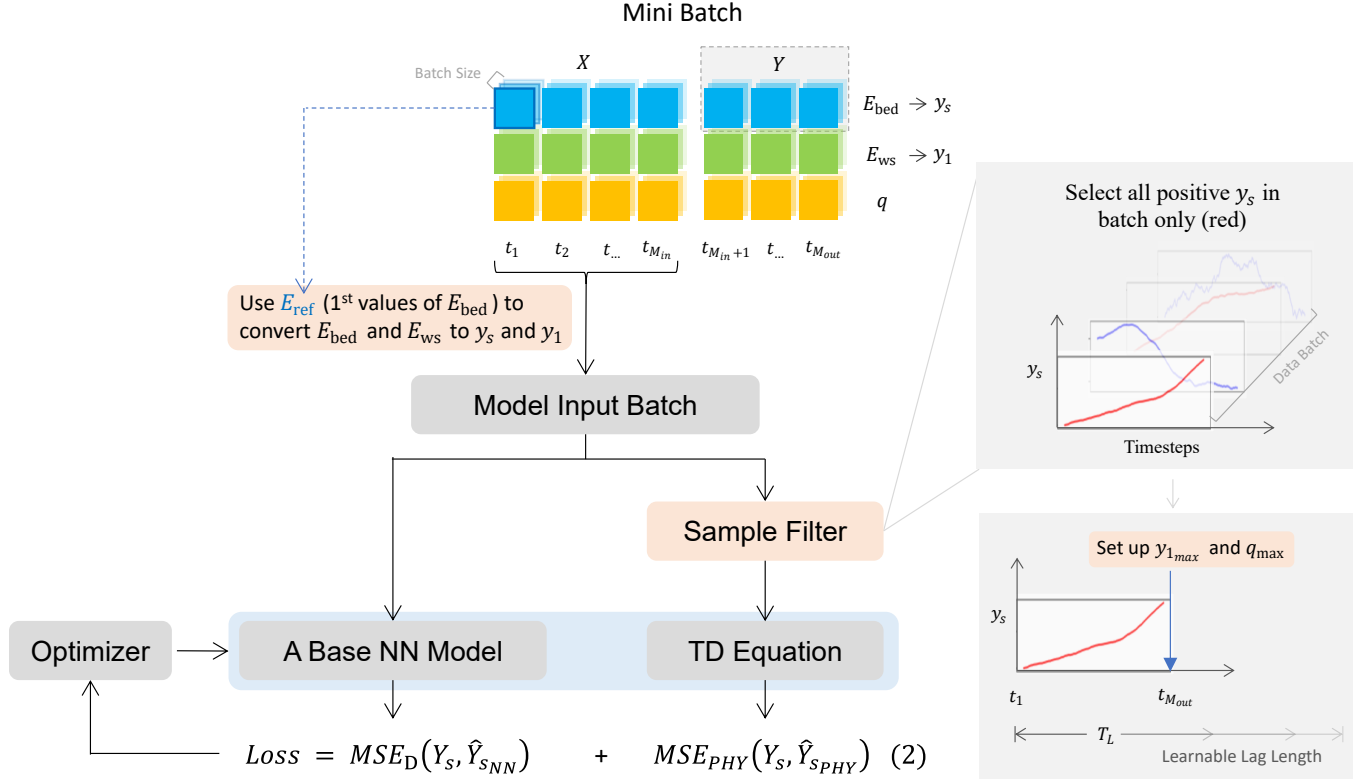


Fig. 4. The training process of the time-dependent SPINN model, which incorporates scouring episode detection and applies the physical loss term only during scouring episodes.

similarities), we introduce SPINN-GTD by eliminating all site-specific parameters from the SPINN-TD empirical equation (Equation 8), as outlined in Equation 9:

$$\hat{y}_{st} = p_1 (y_{1max})^{-\alpha} (q_{max})^{\beta} \left(1 - e^{-\frac{t}{T_L}}\right) \quad (9)$$

where α and β represent hyperparameters introduced to offer more flexibility in the shape of the empirical model to adjust to a range of bridges.

This approach enables the SPINN model to get trained with a much larger database and learn the features of a wider range of scour events from a cluster of bridges showing similar flow and scour trends. Such transferable model is envisaged to be able to collate and transfer the learning among several bridges. Transferable models are particularly relevant for new bridges with limited data available. The calibrated general time-dependent (GTD) equation may be viable to provide reasonable estimates of maximum scour depth in a new bridge within the same region/cluster. We evaluated this hypothesis in the following sections.

2.3.4 Base DL Algorithm: 1-Long Short-Term Memory Networks (LSTM)

LSTM is a type of recurrent neural network (RNN) that excels in capturing and modelling temporal dependencies within time series/sequential data (Hochreiter and Schmidhuber, 1997). A critical challenge in training deep neural networks is the vanishing gradient problem, where gradients shrink to a very small

level during back-propagation, which hinders effective learning. LSTM networks address this problem through their unique gate mechanisms, which regulate and maintain the gradient flow, preventing its significant diminish across the network's layers. The strength of LSTMs lies in their ability to remember long-term dependencies in sequential data, allowing them to capture complex patterns that traditional models might miss. This feature is particularly advantageous in time series prediction, where future outcomes are influenced not just by recent events but also by occurrences in the distant past, resulting in more accurate and robust predictions.

In this study, we implement a one-layer LSTM model with 128 hidden units as shown in Fig. 5. The input sequence is processed by the LSTM layer, and then passed through a dense (fully connected) layer with a linear activation function and finally reshaped into the output sequence.

Readers are referred to [Yousefpour and Correa \(2023\)](#) and [Hashem and Yousefpour \(2024\)](#) for more details on optimisation and hyperparameter tuning for the LSTM scour models.

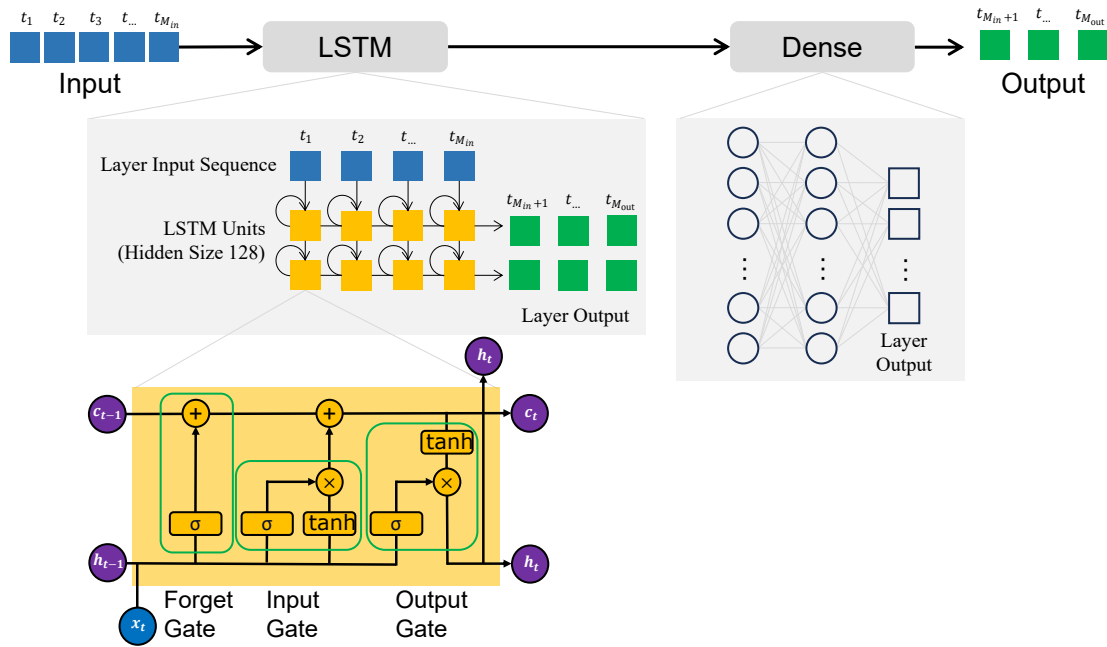


Fig. 5. The architecture of LSTM base models for SPINNs, showing the LSTM Memory Unit gates and the input (x_t), hidden (h_t), and cell state (c_t) vectors.

2.3.5 Base DL Algorithm: 2-Convolutional Neural Network (CNN)

CNN is one of the most prevalent types of neural network applied in computer vision due to its effectiveness in learning image features ([Venkatesan and Li, 2017](#)). In recent years, they have also found applications in time series prediction tasks, where the inputs are structured as sequential data ([Livieris et al., 2020](#)). Similar to spatial pattern identification in images, CNN can also be adapted to capture temporal patterns and dependencies within sequential data in the context of time series prediction ([Liu et al., 2022](#)).

In this study, we develop a CNN model with two 2D convolutional layers to show the adaptability of CNNs for processing multidimensional time series data. The two CNN layers have a kernel size of 5, padding size of 2, and output sizes of 128 and 256, respectively. Also, batch normalization layers are

added after these layers, and one following dense layer is responsible for producing the final prediction. The CNN model architecture is shown in Fig. 6.

Readers are referred to [Hashem and Yousefpour \(2024\)](#) for details of model optimisation and hyperparameter tuning for the CNN models.

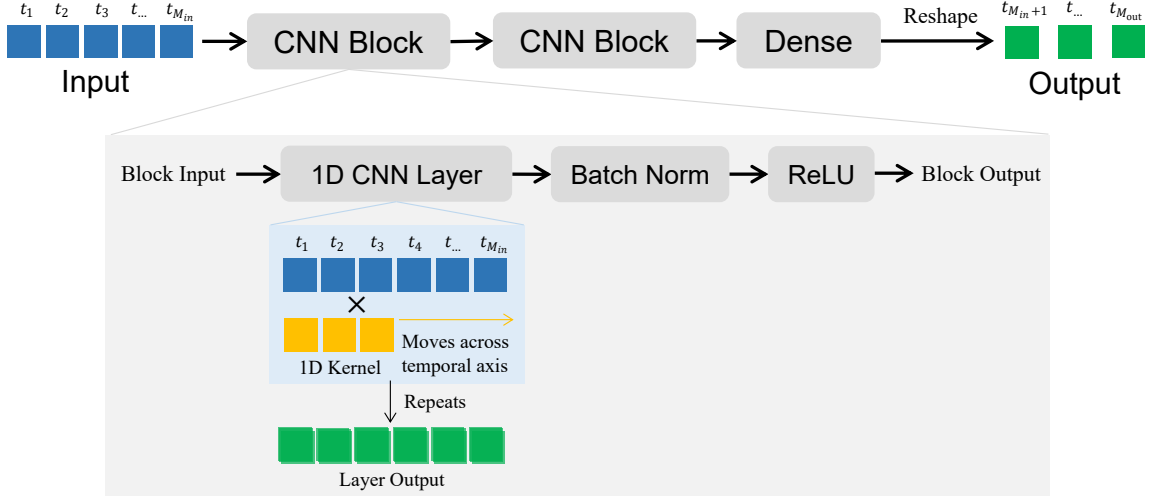


Fig. 6. The architecture of the base CNN models for SPINNs.

3 Results and Discussion

3.1 Experimental Design

A number of experiments were performed to evaluate the performance of the three SPINN variants and their counterpart pure NN (base data-driven) models. The experiments can be categorized into general/transferrable and site/bridge-specific as shown in Table 3.

The models trained using bridge-specific data will be evaluated with the corresponding test set, while the model trained on all bridges will be evaluated individually for each of the four bridges. Considering the stochastic nature inherent in NN modelling, each experiment is trained and evaluated five times to ensure the robustness of the results. The averaged MSE values over the validation and test datasets are used to evaluate the performance of models.

In addition to MSE, we also use Mean Absolute Percentage Error (MAPE) and Root Mean Squared Error (RMSE) as performance metrics for evaluating the models. MAPE and RMSE are defined as:

$$MAPE = \frac{1}{M_{out}} \sum_{i=0}^{M_{out}} \left| \frac{y_i - \hat{y}_i}{y_i} \right| \times 100 \quad (10)$$

$$RMSE = \sqrt{\frac{1}{M_{out}} \sum_{i=0}^{M_{out}} (y_i - \hat{y}_i)^2} \quad (11)$$

Table 3. Experiment design for evaluation of SPINN variants and their corresponding pure data-driven models. The general models trained using a combination of all four datasets indicated as "All". The latent parameters calibrated through the SPINN training process are highlighted.

Experiments	Training Dataset	Base Data-Driven Model	\hat{Y}_{SPHY}
Pure NN (Site-Specific)	212	LSTM	N/A
	527	CNN	
	539		
	742		
Pure NN (General)	All	LSTM	N/A
		CNN	
SPINN-HEC18 (Site-Specific)	212	LSTM	$p_1 2.0 K_1 K_2 K_3 \frac{a^{0.65}}{g^{0.215} L^{0.43} y_1^{0.295}} \left(\frac{q}{p_2}\right)^{0.43}$
	527	CNN	
	539		
	742		
SPINN-TD (Site-Specific)	212	LSTM	$p_1 2.0 K_1 K_2 K_3 \frac{a^{0.65}}{g^{0.215} L^{0.43} y_{1max}^{0.295}} \left(\frac{q_{max}}{p_2}\right)^{0.43} \left(1 - e^{-\frac{p_3 \times t}{T_L}}\right)$
	527	CNN	
	539		
	742		
SPINN-GTD (General)	All	LSTM	$p_1 (y_{1max})^{-\alpha} (q_{max})^{\beta} \left(1 - e^{-\frac{t}{T_L}}\right)$
		CNN	

where y_i is the actual scour depth and \hat{y}_i is the predicted scour depth at timestep i .

The models were implemented using PyTorch (Paszke et al., 2017) python packages and were run on 4 NVIDIA A100 Tensor Core GPUs and 2×16 Core CPUs on the *Geo&Co* Infrastructure Department High-Performance Computing Center at the University of Melbourne.

3.2 DL Model Configuration and Training

Fig. 7 shows the historical time series data of Bridge 539 as an example (see Appendix Section for time series data for other case study bridges). Multiple data gaps are found within the data, which is mainly seasonal freezing in Alaska. We use a sliding window with a length equal to M_{in} plus M_{out} to slice the data into the sequences for training.

Based on the top model configurations identified through comprehensive hyperparameter tuning performed by Yousefpour and Correa (2023) and Hashem and Yousefpour (2024), the input width, M_{in} and output/label width, M_{out} for all models are set to 168 hours (seven days). This means that after training the models with the historical time series data up to the current time, the last one-week data is used as input to predict the scour depth for the coming week.

For each bridge, we have time series data across several years. We create input-output pairs by sliding a

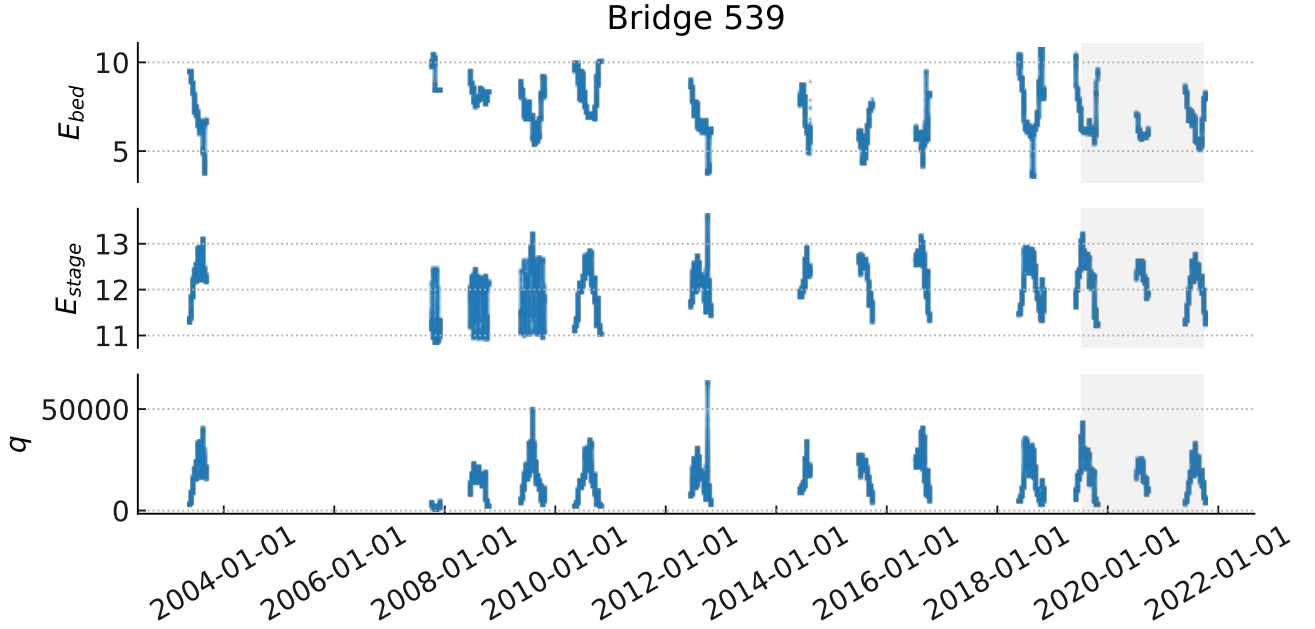


Fig. 7. Historical time series data for Bridge 539 shows the three features: bed elevation (m), river stage elevation (m), and discharge (m^3/s). The grey zone shows the test subset, and the transparent part before is the training and validation subsets.

Table 4. The split of training, validation, and testing sets for each bridge.

Bridges	Type	Start	End	No. of Sequences
212	Train/Validation	2012-06-05 13:00	2017-08-06 02:00	11,573
212	Test	2017-08-06 03:00	2018-09-27 03:00	2725
527	Train/Validation	2005-06-02 15:00	2019-06-11 11:00	41,473
527	Test	2019-06-11 12:00	2021-09-25 22:00	9782
539	Train/Validation	2003-05-13 17:00	2019-07-10 17:00	29,626
539	Test	2019-07-10 18:00	2021-09-25 20:00	7155
742	Train/Validation	2013-05-27 02:00	2017-07-09 23:00	7,462
742	Test	2017-07-10 00:00	2017-09-11 17:00	1,530

window over the continuous time series data, resulting in a number of data slices. We arrange these slices in temporal order and allocate the last 20% for the test set. The first 80% of the samples are then randomly split into training and validation sets in a 3:1 ratio (60% for training and 20% for validation). The model is validated after each training epoch to monitor its performance on unseen data and prevent overfitting. The range of available time series data and the number of available sequences over training/validation and test datasets in each bridge is provided in Table 4. Fig. 7 illustrates the data split for Bridge 539. Similar illustrations for other bridges can be found in the Appendix Section (Figs. A1 to A3).

3.3 DL Model Performance Variation Across Case Studies

Fig. 8 presents the boxplots of performance (MSE) for all models over the test dataset. The detailed performance of all variants is provided in Table A1. The aggregated MSE of five runs is listed as the mean and standard deviation values for each model.

Table 5 presents the MAPE and MSE criteria for pure data-driven models across case study bridges. It is shown that the order of performance across four bridges is different for the two performance criteria. MAPE is a percentage-based metric that provides insights into the relative magnitude of errors and is particularly useful when comparing models across bridges with varying scales of bed elevations. On the other hand, MSE concentrates larger errors by squaring them, making it more sensitive to outliers. Also, the trend in model performance across different bridges does not show a correlation with the amount of training data available for each bridge (see Table 4).

The DL model performance for each bridge can be influenced by data quality, scale of variation, amount of missing data, and consistency in seasonal and temporal patterns across years. As observed in Fig. 7, and also Fig. A1 to A3, the degree of fluctuations in the bed elevation, E_{bed} , varies across case study bridges. For instance, Bridge 539 experienced several significant scour events across the years, with some scour depths reaching over five meters. In contrast, bed elevation changes at Bridge 527 were small, with variations consistently below two meters. Similarly, bridge 212 does not show significant scour and filling throughout the years. It should be noted that this variability in scale and rate of variation in scour depth can affect the relative performance of different DL algorithms. This complexity should be acknowledged in comparing and assessment of competing models.

Table 5. Performance of site-specific and general pure data-driven models for four case study bridges, showing MSE (m^2) / MAPE (%) values. Elev. represents the maximum bed elevation variation (m) over the test dataset.

	Elev.	Pure-LSTM		Pure-CNN	
		Site-Specific	General	Site-Specific	General
212	0.644	0.533/0.069	0.089/0.034	0.142/0.041	0.101/0.033
527	2.030	0.141/0.010	0.113/0.010	0.055/0.006	0.123/0.010
539	4.603	0.478/0.537	0.332/0.546	0.283/0.406	0.276/0.485
742	3.191	0.884/0.127	0.325/0.111	0.214/0.079	0.310/0.106

3.4 Assessment of SPINN Variants

SPINNs show improvement in predictive accuracy compared with pure NN models in majority of cases. As observed from Fig. 8, SPINNs help with reducing mean error and/or reducing the standard deviation of error for 9 out of 16 experiments (4 bridges, 2 base models, site-specific and general). Refer to Table A1 for a summary of performance (MSE) from all cases/experiments. Table 6 provides mean and standard deviation of MSE for SPINN variants versus their corresponding pure NN models for bridge 539 and 742.

For the site-specific category, the SPINN variants showed considerably better performance compared to their pure NN counterparts for the LSTM group. In the case of Bridge 539 for instance, the SPINN-TD variant reduces the MSE by 50% (from 0.48 to $0.24m^2$). The SPINN-HEC18 variant also enhances the performance of LSTM by 19% (from 0.48 to $0.39 m^2$). Similarly, for Bridge 742, the SPINN-TD variant

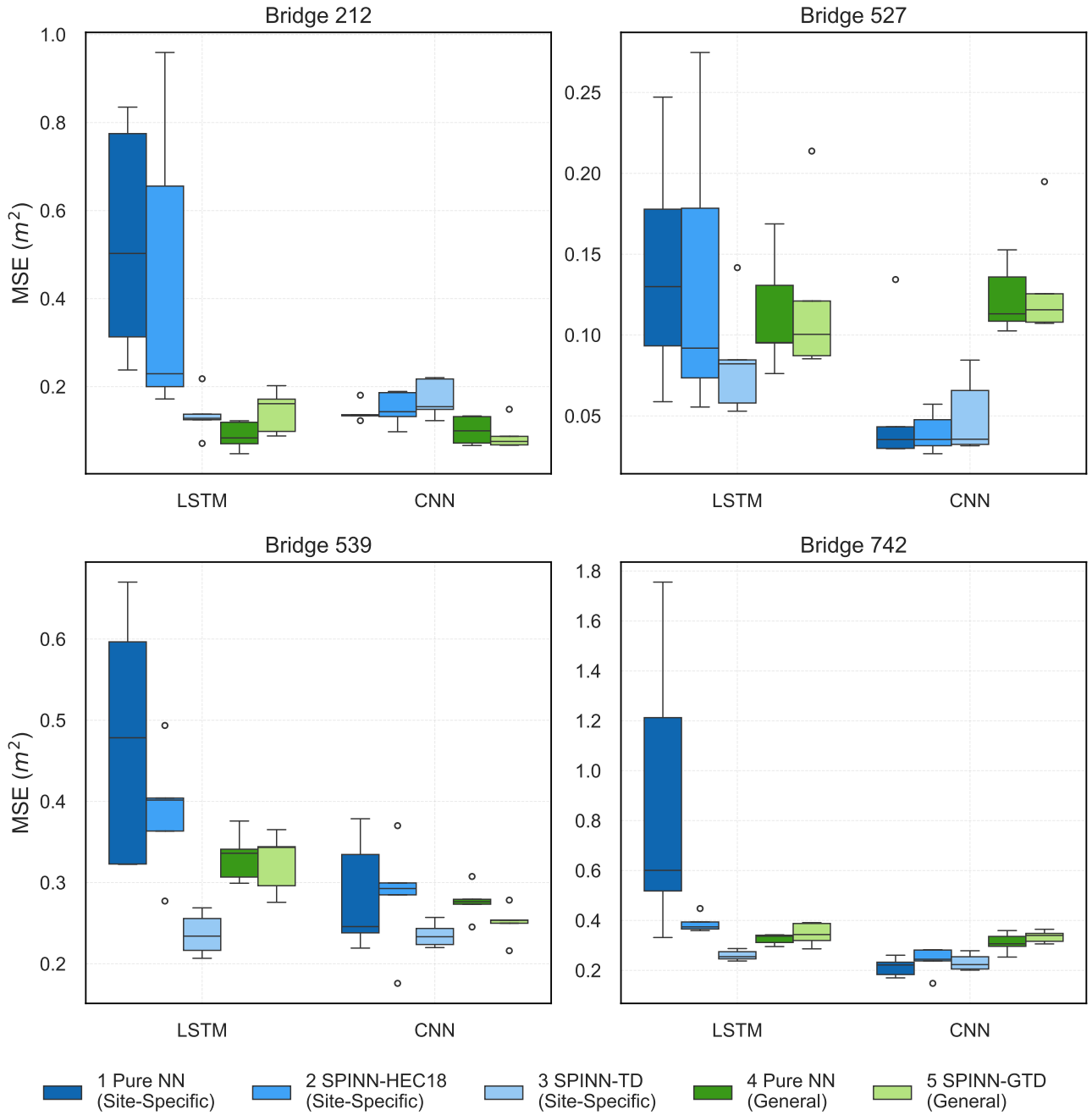


Fig. 8. Model performance across four case study bridges, showing the test MSE (m^2) boxplots for site-specific (blue) and general (green) Pure NN and SPINN variants.

reduces the error by 70% (MSE from 0.88 to $0.26m^2$) for the LSTM base model. In CNN group, for bridge 539, SPINN-TD reduces the MSE by 17% (from 0.28 to $0.24m^2$), however, for the other three bridges SPINN variants and pure CNN models show close performance with MSE average less than $0.3m^2$.

For the general/transerable models, SPINN-GTD shows comparable performance with marginal improvement. The best outcome is observed for the CNN model of bridge 539 with 9% (from 0.276 to 0.250)

MSE reduction.

Table 6. Performance of SPINN variants and Pure NN models, showing MSE (m^2) in bed elevation prediction over test datasets for Bridges 539 and 742.

Model	Training Datasets	Method	MSE - 539	MSE - 742
LSTM	Site Specific	Pure NN	0.478±0.157	0.884±0.589
LSTM	Site Specific	SPINN-HEC18	0.388±0.078	0.388±0.036
LSTM	Site Specific	SPINN-TD	0.236±0.026	0.260±0.021
LSTM	General	Pure NN	0.332±0.031	0.325±0.021
LSTM	General	SPINN-GTD	0.325±0.037	0.346±0.045
CNN	Site Specific	Pure NN	0.283±0.069	0.214±0.037
CNN	Site Specific	SPINN-HEC18	0.285±0.070	0.239±0.055
CNN	Site Specific	SPINN-TD	0.236±0.015	0.233±0.033
CNN	General	Pure NN	0.276±0.022	0.310±0.040
CNN	General	SPINN-GTD	0.250±0.022	0.335±0.024

Table 7. Comparison of SPINN variants across four case study bridges, based on MSE (m^2) values. Elev. represents the maximum bed elevation variation (m) over the test dataset.

	Elev.	SPINN-HEC18		SPINN-TD		SPINN-GTD	
		LSTM	CNN	LSTM	CNN	LSTM	CNN
212	0.644	0.443	0.150	0.136	0.173	0.144	0.089
527	2.030	0.135	0.040	0.084	0.050	0.122	0.130
539	4.603	0.388	0.285	0.236	0.236	0.325	0.250
742	3.191	0.388	0.239	0.260	0.233	0.346	0.335

Table 7 compares the performance of different SPINN variants across the four case study bridges. The SPINN-TD model consistently outperforms the other SPINN variants, achieving the lowest MSE for most of the bridges when paired with LSTM and CNN base models. This suggests that incorporating the proposed site-specific time-dependent equation (TD) as a physics-based loss function is more effective compared to the site-specific HEC18 and the generalized version of the TD equation (GTD). However, the degree of performance improvement varies depending on the specific bridge and base NN model. For instance, while SPINN-TD shows significant error reduction for Bridge 539 when paired with LSTM (50% reduction) and CNN (17% reduction), the improvement is less pronounced for Bridge 527 with the same base models (40% and 9% reduction, respectively). This variability in performance gain suggests that the effectiveness of the physics-based loss functions is influenced by the inherent characteristics of each bridge dataset.

3.5 Site-Specific vs General/Transferable DL Models

The general pure data-driven models (Pure NN) show better performance (lower MSE and lower standard deviation) compared to site-specific models, except for CNN in the case of Bridge 212 and 539

(see Table 5 and Fig. 8). For instance, training the LSTM model with the combined datasets from all bridges led to $\sim 60\%$ and $\sim 80\%$ reduction in MSE for bridges 742 and 212, respectively. It is noted that these two bridges had less amount of site-specific data. This indicates aggregating data from a cluster of similar bridges can potentially enhance the generalization of the DL models. This outcome highlights the potential for developing transferable scour forecast models applicable to a cluster of bridges in a region.

However, the general hybrid models, that is, SPINN-GTD did not show consistent superiority over site-specific hybrid models, i.e. SPINN-HEC18 or SPINN-TD (except for 539 LSTM, 742 LSTM, 212 CNN cases). The challenge of transferability in the SPINN-GTD model is that the general empirical equation is being fit to a wider range of scour characteristics. The GTD equation in fact combines all the site/bridge-specific coefficients and inputs of the site-specific TD equation (i.e., riverbed, flow and pier shape/dimension factors) into one latent parameter (p_1). This could limit the extent to which the empirical model can help NN learn and adapt adequately to the inherent scour patterns for each bridge, thus reducing the prediction accuracy.

3.6 Evaluation of Base DL Algorithms for SPINNs

As shown in Table 5 the relative performance of pure DL models varies across bridges, however, CNN seems to overall outperform LSTM in prediction accuracy, however not in computational cost as shown in Table 8.

The comparison of computational cost between LSTM and CNN is expressed in terms of Floating Point Operations (FLOPs). In deep learning, FLOPs are estimated by counting the total number of multiplication and addition operations required for one forward pass through the model. The number of trainable parameters reflects the model’s capacity to learn from data, while FLOPs demonstrate the computational demand for training.

Table 8. Latent Parameters and FLOPs for Different Models.

Model	Trainable Parameters	FLOPs
LSTM	3,681,448	22,966,272
CNN	7,393,704	42,513,408

As shown in Table 8, there is a direct correlation between the model’s complexity and its computational cost. The CNN architecture requires approximately twice the computational effort of the LSTM due to its complex convolutional layers. Regarding the SPINN framework, HEC18, TD, and GTD only introduce a few latent parameters to the base NN (See Table 3), thereby leading to a negligible extra computational cost. This enables SPINN variants to leverage the benefits of physics-inspired learning without incurring a substantial computational burden.

LSTM shows to achieve significant performance improvement in terms of accuracy (error) and robustness (variance) from a physics-inspired architecture. Given the variability of scour data in various bridges, it is important to investigate competing NN base models to achieve the most optimal performance.

3.7 Forecasting Trends and Capturing Scour Events

The primary objective of the scour forecasting model lies in its ability to predict major scour and filling events in advance. Fig. 9 and Fig. 10 present the SPINN model predictions over the test dataset for the

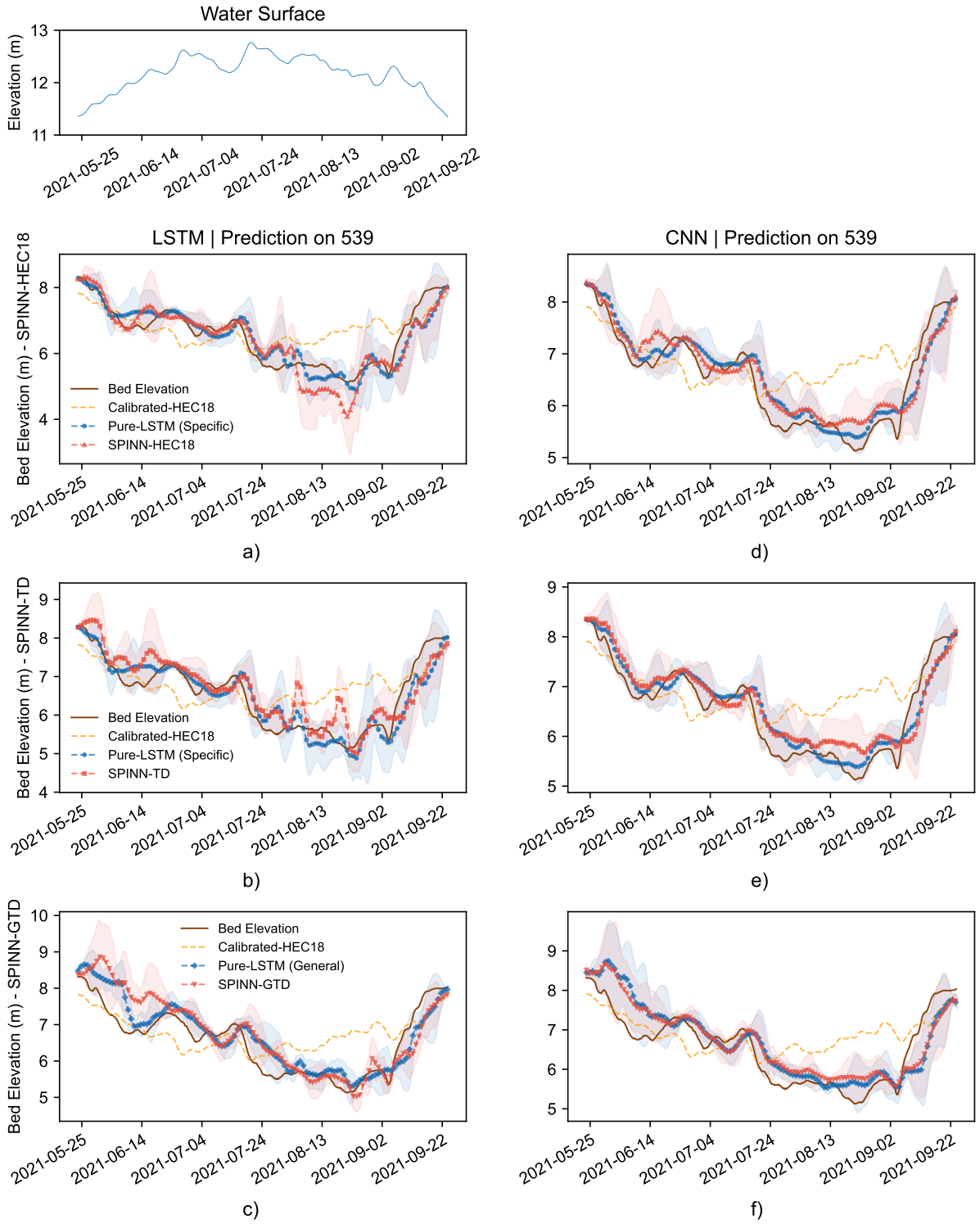


Fig. 9. Model predictions versus actual observations for Bridge 539 test set (May-September 2021). Top graph displays the flow changes in this period. (a-c) show LSTM-based predictions, (d-f) display CNN-based predictions, and each row represents SPINN-HEC18, SPINN-TD, and SPINN-GTD, respectively. Additional test periods are presented in the Appendix.

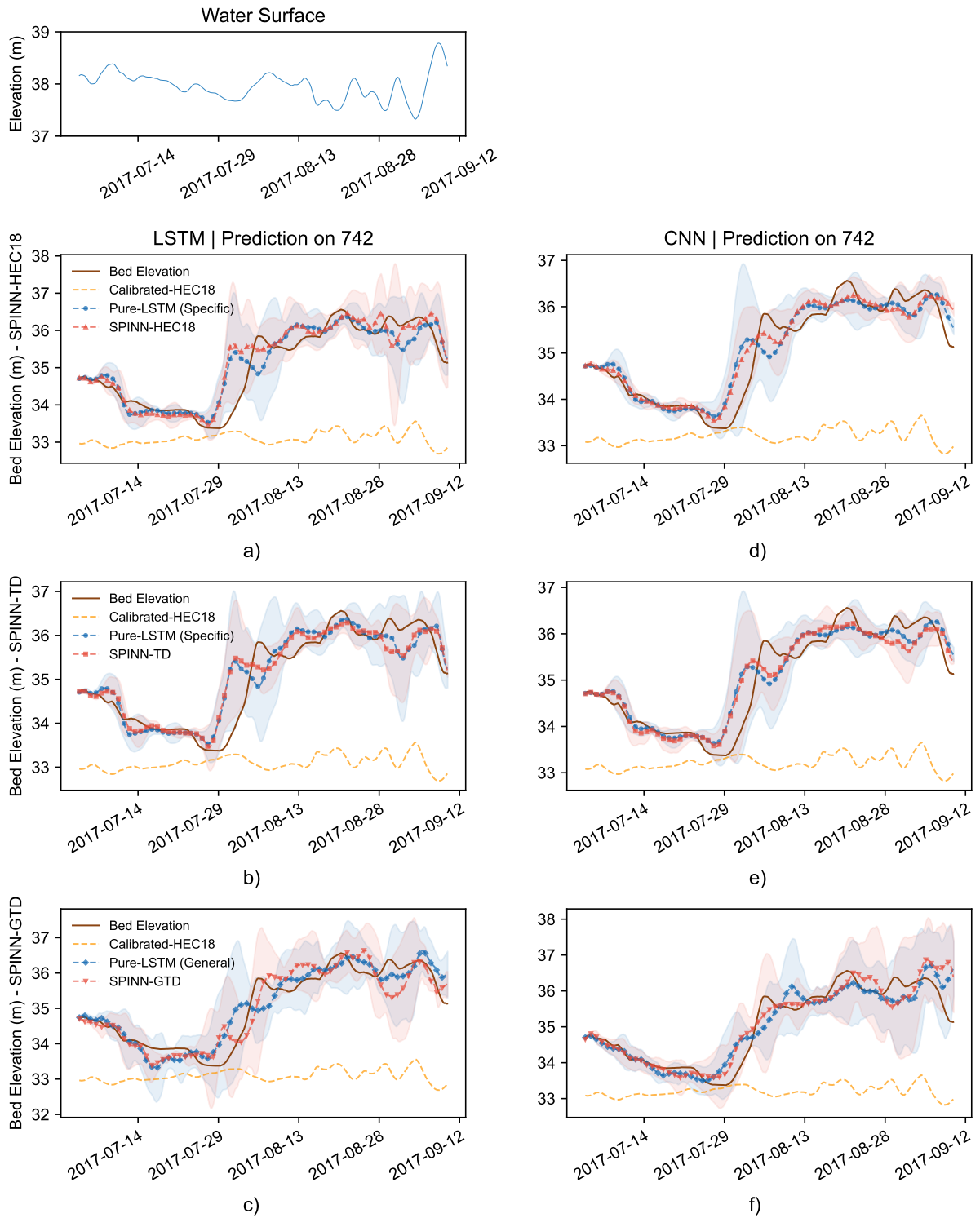


Fig. 10. Model predictions versus actual observations for Bridge 742 test set (July-September 2017). Top graph displays the flow changes in this period. (a-c) show LSTM-based predictions, (d-f) display CNN-based predictions, and each row represents SPINN-HEC18, SPINN-TD, and SPINN-GTD, respectively.

three SPINN models. Due to relatively stable bed elevation in the test sets of Bridge 212 and 527, our analysis here is focused on Bridges 539 and 742. The actual river bed elevation changes are depicted as a solid brown line, while the model predictions are shown as dashed lines. The predictions using pure NN models and the calibrated HEC18 empirical equation (CEE-SPINN-HEC18) derived from SPINN (see Section 3.8) are used as baselines for comparison (see also Table 6).

Comparing both data-driven and hybrid-physics-data-driven models with the calibrated HEC18 equation (CEE-SPINN-HEC18) shows the superiority of the DL models for scour prediction compared with an empirical model. The calibrated HEC-18 model struggles to follow the scouring and filling trends and significantly underestimates the scour depth in most periods for bridges 539 and 742 (see Figs. 9 and 10).

3.8 The SPINN-Calibrated Empirical Equations

In this section, we shift the focus towards the calibrated empirical equations derived from the proposed SPINN framework. We will evaluate the performance of the three calibrated equations (see Table 3) and assess their potential to be implemented as independent scour models.

Since the empirical equations are designed to predict maximum scour depth, their performance is only evaluated during scouring episodes. Bridge 539 paired with the LSTM group is chosen here as an example for detailed analysis, considering the deeper scouring depth and the superior performance of the base model.

Fig. 11 displays the training progress plots of the latent parameters incorporated in the three empirical equations over 500 training epochs. The parameter p_1 in all equations acts as an overall adjustment factor, converging to distinct values for each equation, indicating its role in tailoring the output of each empirical equation. The p_2 in HEC18 and TD, representing the adjustment on the velocity, stabilizes at 1.0 after initial training epochs, suggesting its impact may be mitigated by adjustments in p_1 . Similarly, p_3 in TD converges to 1.0, reflecting its minimal influence on the final results. T_L is calibrated to various values for site-specific models and to 2.3 hrs for the general model. The summary of calibrated parameters across different scenarios can be found in Table 9.

Table 9. The calibrated equation parameters from SPINN models.

Bridge	Equation	p_1	p_2	p_3	T_L (hour)	α	β
212	HEC18	2.480	1.000	N/A	N/A	N/A	N/A
212	TD	0.534	1.000	1.000	1.970	N/A	N/A
527	HEC18	0.371	1.000	N/A	N/A	N/A	N/A
527	TD	0.098	1.000	1.000	0.356	N/A	N/A
539	HEC18	1.790	1.000	N/A	N/A	N/A	N/A
539	TD	0.514	1.000	1.000	1.750	N/A	N/A
742	HEC18	1.350	1.000	N/A	N/A	N/A	N/A
742	TD	0.329	1.000	1.000	9.470	N/A	N/A
All	GTD	0.076	N/A	N/A	2.290	0.903	0.592

Fig. 12 compares the calibrated empirical equations (CEE) derived from the SPINN model for predicting maximum scour depth on the Bridge 539 test dataset. The actual bed elevation changes are highlighted with a solid brown line, while the predictions from the CEEs are marked with dashed lines. The CEE-SPINN-TD

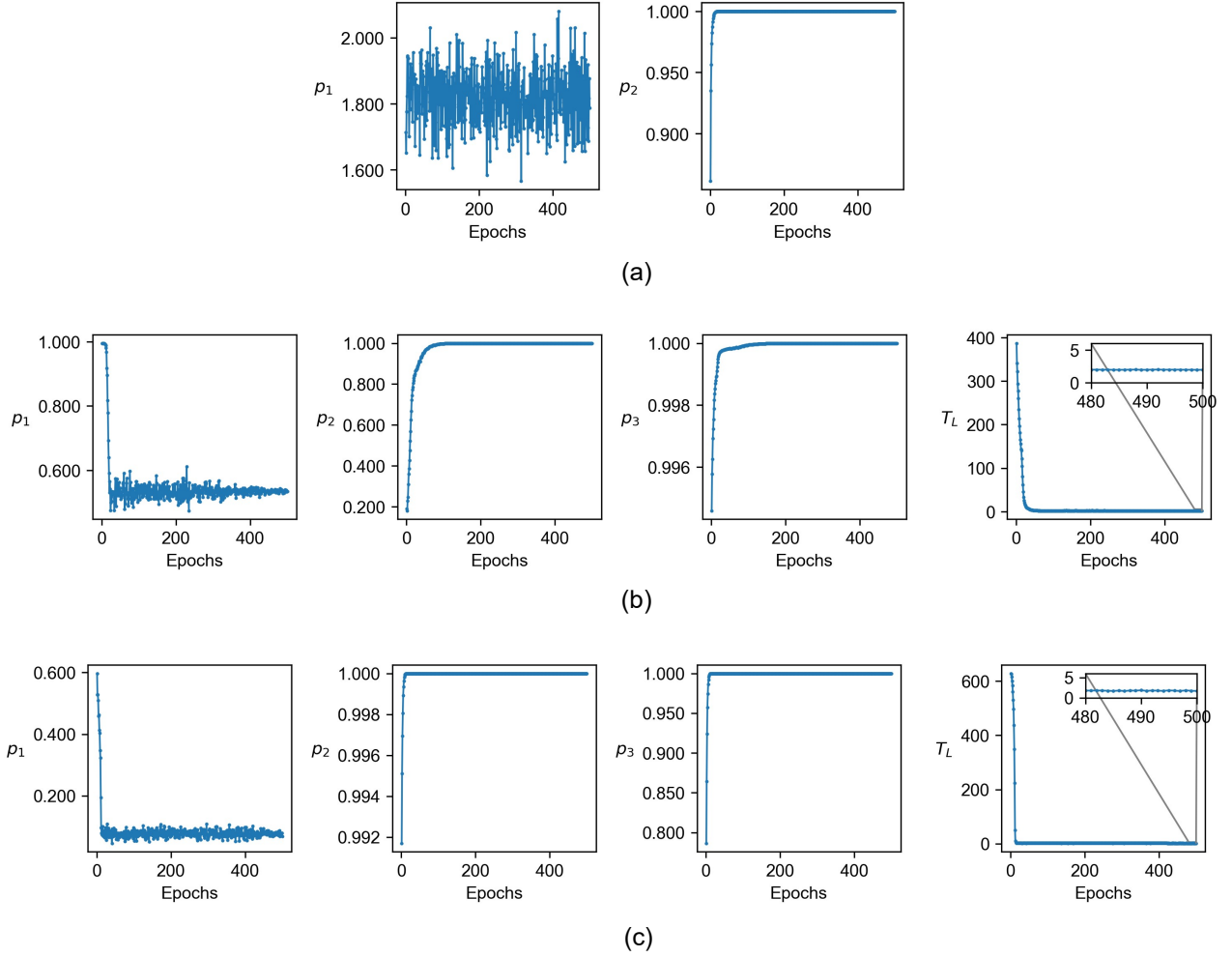


Fig. 11. The calibration of empirical equations with LSTM SPINN model, using the 539 dataset for site-specific models (GTD uses all datasets). a) The latent parameters of the HEC18 equation, b) The latent parameters of the TD equation, and c) The latent parameters of the GTD equation.

and CEE-SPINN-GTD employ time-dependent equations, where an exponential function predicts the scour depth for each timestep in the scouring episode. The predicted depth is zero at the beginning of the episode ($t = 0$) and reaches the maximum scour depth ($y_{s_{max}}$) at a time close to the calibrated time lag parameter (T_L). On the other hand, the CEE-SPINN-HEC18 uses the same dynamic reference level approach as the time-dependent equations to estimate the maximum scour depth of each episode (horizontal dashed line).

Among the CEEs calibrated through SPINN, the HEC18 overestimates the maximum scour depth by up to 3 meters. Across these scouring episodes in Fig. 12, the CEE-SPINN-HEC18, CEE-SPINN-TD, and CEE-SPINN-GTD yield RMSEs (m) of 2.539, 0.443, and 0.34 respectively. Although not as accurate as SPINN models, the proposed SPINN-calibrated time-dependent empirical equations show great potential to replace existing empirical models for maximum scour depth estimation.

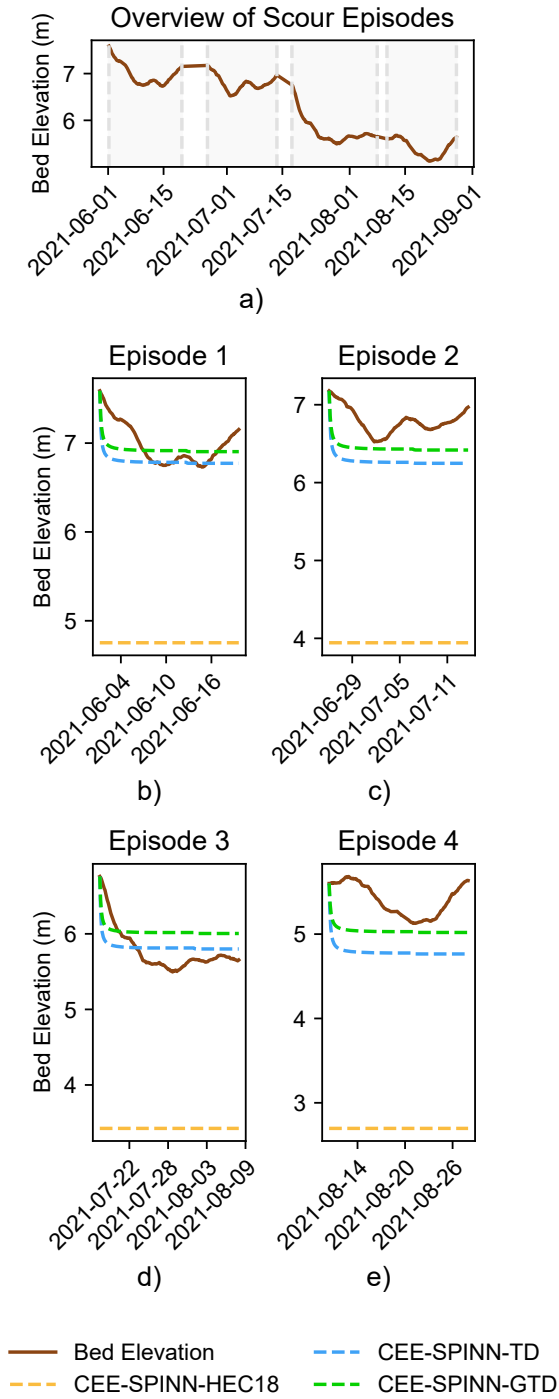


Fig. 12. Maximum scour prediction using the calibrated empirical models (CEE) for Bridge 539, a) the overview of bed elevation changes; (b-e) prediction on each scour episode using three SPINN-calibrated equations.

4 Conclusion

This paper introduced scour physics-inspired neural network algorithms, SPINNs, exploring hybrid physics-data-driven models for bridge scour prediction based on deep learning. Central to SPINN’s methodology

is the integration of physics-based empirical equations as supplementary loss components into deep neural networks. Although SPINNs performance showed variability with the choice of base DL model, the empirical equation and the case study bridge, they showed superior performance in the majority of scenarios compared to pure data-driven (NN) models. The bridge-specific variants of SPINN with the proposed time-dependent (TD) empirical equation showed the most competitive performance among other SPINN variants. For some scenarios, such as the LSTM group for Bridge 539, the SPINN could help the base NN model reduce forecasting error by up to 50%.

We explored the idea of transferable models for bridge clusters by aggregating bridge datasets across a cluster to train general DL models that can provide reasonable scour prediction for any bridge within that cluster. The general pure data-driven (NN) models showed superiority over site-specific models, however, the general SPINN with the proposed empirical model did not provide as accurate predictions as site-specific SPINNs.

This study revealed that the sister calibrated empirical equations derived from SPINN framework, particularly the introduced time-dependent equation, can provide a viable alternative to traditional scour models, such as FHWA HEC-18. As opposed to traditional HEC-18, which is often calibrated using discrete scour lab measurements, the empirical equations within SPINN are calibrated using historical time series of scour monitoring data throughout the neural network training process. The proposed general time-dependent calibrated equation can be particularly helpful in scenarios where site-specific flow and riverbed conditions are not readily available (e.g., in new bridge projects).

Comparing SPINNs and the SPINN-calibrated empirical equations with traditional empirical models presents a significant improvement, which can benefit the current state of practice in bridge scour design and management. This paper can pave the path for future studies on physics-inspired machine learning for scour prediction.

5 Data Availability Statement

Some or all data used for this study are available from the corresponding author upon request. Models or codes generated or used during the study are proprietary or confidential in nature and may only be provided with restrictions. Related data and codes are available at <https://github.com/Data-Driven-Computational-Geotechnics/ScourSensePhase4/>.

6 Acknowledgments

This research was supported by The University of Melbourne’s Spartan and the GEO&CO Infrastructure HPC Center. The funding was provided by The University of Melbourne’s Start-Up awarded to Dr Negin Yousefpour.

References

Amini, D., Haghghat, E., and Juanes, R. (2023). “Inverse modeling of nonisothermal multiphase poromechanics using physics-informed neural networks.” *Journal of Computational Physics*, 490.

- Arneson, L., Zevenbergen, L., Lagasse, P., and Clopper, P. (2012). *Evaluating Scour at Bridges-Fifth Edition, Hydraulic Engineering Circular No. 18*. Federal Highway Administration (FHWA) (April).
- Briaud, J.-L., Hurlabaus, S., Chang, K., Yao, C., Sharma, H., Yu, O.-Y., Darby, C., Hunt, B., and Price, G. (2011). “Real-time monitoring of bridge scour using remote monitoring technology.” *Rep. No. 0-6060-1*, Texas A&M University/TTI.
- Briaud J.L., Medina-Cetina Z., Hurlabaus S., Everett M., Tucker S., Yousefpour N., and Arjwech R. (2012). “Unknown foundation determination for scour.” *Report no.*, Texas A&M University, College Station (8).
- Chen, J. and Liu, Y. (2021). “Probabilistic physics-guided machine learning for fatigue data analysis.” *Expert Systems with Applications*, 168.
- Chen, Y., Xu, Y., Wang, L., and Li, T. (2023). “Modeling water flow in unsaturated soils through physics-informed neural network with principled loss function.” *Computers and Geotechnics*, 161.
- Eghbalian, M., Pouragha, M., and Wan, R. (2023). “A physics-informed deep neural network for surrogate modeling in classical elasto-plasticity.” *Computers and Geotechnics*, 159.
- Faroughi, S. A., Pawar, N. M., Fernandes, C., Raissi, M., Das, S., Kalantari, N. K., and Mahjour, S. K. (2024). “Physics-guided, physics-informed, and physics-encoded neural networks and operators in scientific computing: Fluid and solid mechanics.” *Journal of Computing and Information Science in Engineering*, 24.
- Haghighat, E., Raissi, M., Moure, A., Gomez, H., and Juanes, R. (2021). “A physics-informed deep learning framework for inversion and surrogate modeling in solid mechanics.” *Computer Methods in Applied Mechanics and Engineering*, 379.
- Hashem, T. and Yousefpour, N. (2024). “Application of long-short term memory and convolutional neural networks for real-time bridge scour forecast.
- Hochreiter, S. and Schmidhuber, J. (1997). “Long short-term memory.” *Neural computation*, 9(8), 1735–1780.
- Jia, X., Willard, J., Karpatne, A., Read, J. S., Zwart, J. A., Steinbach, M., and Kumar, V. (2021). “Physics-Guided Machine Learning for Scientific Discovery: An Application in Simulating Lake Temperature Profiles.” *ACM/IMS Transactions on Data Science*, 2(3).
- Karniadakis, G. E., Kevrekidis, I. G., Lu, L., Perdikaris, P., Wang, S., and Yang, L. (2021). “Physics-informed machine learning.” *Nature Reviews Physics*.
- Karpatne, A., Atluri, G., Faghmous, J. H., Steinbach, M., Banerjee, A., Ganguly, A., Shekhar, S., Samatova, N., and Kumar, V. (2017). “Theory-guided data science: A new paradigm for scientific discovery from data.” *IEEE Transactions on Knowledge and Data Engineering*, 29.
- Kingma, D. P. and Ba, J. (2014). “Adam: A method for stochastic optimization.” *arXiv preprint arXiv:1412.6980*.
- Kirby, A., Roca, M., Kitchen, A., Escarameia, M., and Chesterton, O. (2015). *Manual on scour at bridges and other hydraulic structures*. Ciria.
- Lan, P., jing Su, J., yan Ma, X., and Zhang, S. (2024). “Application of improved physics-informed neural networks for nonlinear consolidation problems with continuous drainage boundary conditions.” *Acta Geotechnica*, 19.
- Li, K. Q., Yin, Z. Y., Zhang, N., and Li, J. (2024a). “A pinn-based modelling approach for hydromechanical behaviour of unsaturated expansive soils.” *Computers and Geotechnics*, 169.
- Li, Y., Pan, Y., and Zhang, L. (2024b). “Physics-guided deep learning for driving force estimation in synchronous tunnel boring machines under missing cylinders.” *Automation in Construction*, 161.
- Liang, B., Du, S., Pan, X., and Zhang, L. (2019). “Local scour for vertical piles in steady currents: Review of mechanisms, influencing factors and empirical equations.” *Journal of Marine Science and*

Engineering, 8(1), 4.

- Liu, M., Zeng, A., Chen, M., Xu, Z., Lai, Q., Ma, L., and Xu, Q. (2022). “Scinet: Time series modeling and forecasting with sample convolution and interaction.” *Advances in Neural Information Processing Systems*, 35, 5816–5828.
- Livieris, I. E., Pintelas, E., and Pintelas, P. (2020). “A cnn-lstm model for gold price time-series forecasting.” *Neural computing and applications*, 32, 17351–17360.
- Masi, F. and Einav, I. (2024). “Neural integration for constitutive equations using small data.” *Computer Methods in Applied Mechanics and Engineering*, 420.
- Ngo, H. (2018). *Guide to bridge technology, part 8: hydraulic design of waterway structures*. Number AGBT08-18.
- Paszke, A., Gross, S., Chintala, S., Chanan, G., Yang, E., DeVito, Z., Lin, Z., Desmaison, A., Antiga, L., and Lerer, A. (2017). “Automatic differentiation in pytorch.” *NIPS-W*.
- Pei, T., Qiu, T., and Shen, C. (2023). “Applying knowledge-guided machine learning to slope stability prediction.” *Journal of Geotechnical and Geoenvironmental Engineering*, 149.
- Pizarro, A., Manfreda, S., and Tubaldi, E. (2020). *The science behind scour at bridge foundations: A review*, Vol. 12.
- Raissi, M., Perdikaris, P., and Karniadakis, G. E. (2019). “Physics-informed neural networks: A deep learning framework for solving forward and inverse problems involving nonlinear partial differential equations.” *Journal of Computational Physics*, 378.
- Sheppard, D. M., Demir, H., and Melville, B. W. (2011). *Scour at wide piers and long skewed piers*, Vol. 682. Transportation Research Board.
- Tian, H. and Wang, Y. (2023). “Data-driven and physics-informed bayesian learning of spatiotemporally varying consolidation settlement from sparse site investigation and settlement monitoring data.” *Computers and Geotechnics*, 157.
- Transportation Research Board (TRB) (2009). *Monitoring scour critical bridges*. NCHRP Synthesis of Highway Practice 396, Washington, D.C.
- Venkatesan, R. and Li, B. (2017). *Convolutional neural networks in visual computing: a concise guide*. CRC Press.
- Yousefpour, N. and Correa, O. (2023). “Towards an ai-based early warning system for bridge scour.” *Georisk: Assessment and Management of Risk for Engineered Systems and Geohazards*, 1–27.
- Yousefpour, N., Downie, S., Walker, S., Perkins, N., and Dikanski, H. (2021). “Machine learning solutions for bridge scour forecast based on monitoring data.” *Transportation Research Record*, 2675(10), 745–763.
- Yousif, M. Z., Yu, L., and Lim, H. C. (2022). “Physics-guided deep learning for generating turbulent inflow conditions.” *Journal of Fluid Mechanics*, 936.
- Yu, Y., Yao, H., and Liu, Y. (2020). “Structural dynamics simulation using a novel physics-guided machine learning method.” *Engineering Applications of Artificial Intelligence*, 96.
- Zhang, R., Liu, Y., and Sun, H. (2020). “Physics-guided convolutional neural network (phycnn) for data-driven seismic response modeling.” *Engineering Structures*, 215.
- Zhu, Y., Zabaraz, N., Koutsourelakis, P. S., and Perdikaris, P. (2019). “Physics-constrained deep learning for high-dimensional surrogate modeling and uncertainty quantification without labeled data.” *Journal of Computational Physics*, 394.

Appendix

Table A1. Comprehensive evaluation results of all experiments, comparing the performance of pure NN models and different SPINN variants across four bridge datasets.

Test Set	Base Model	Method	Physics-based Loss	Training Set (s)	Test MSE (m^2)
212	LSTM	Pure NN	N/A	212	0.533±0.267
212	LSTM	Pure NN (General)	N/A	All	0.089±0.032
212	LSTM	SPINN	HEC18	212	0.443±0.350
212	LSTM	SPINN	TD	212	0.136±0.053
212	LSTM	SPINN	GTD	All	0.144±0.049
212	CNN	Pure NN	N/A	212	0.142±0.022
212	CNN	Pure NN (General)	N/A	All	0.101±0.032
212	CNN	SPINN	HEC18	212	0.150±0.039
212	CNN	SPINN	TD	212	0.173±0.044
212	CNN	SPINN	GTD	All	0.089±0.034
527	LSTM	Pure NN	N/A	527	0.141±0.074
527	LSTM	Pure NN (General)	N/A	All	0.113±0.037
527	LSTM	SPINN	HEC18	527	0.135±0.091
527	LSTM	SPINN	TD	527	0.084±0.035
527	LSTM	SPINN	GTD	All	0.122±0.053
527	CNN	Pure NN	N/A	527	0.055±0.045
527	CNN	Pure NN (General)	N/A	All	0.123±0.021
527	CNN	SPINN	HEC18	527	0.040±0.013
527	CNN	SPINN	TD	527	0.050±0.024
527	CNN	SPINN	GTD	All	0.130±0.037
539	LSTM	Pure NN	N/A	539	0.478±0.157
539	LSTM	Pure NN (General)	N/A	All	0.332±0.031
539	LSTM	SPINN	HEC18	539	0.388±0.078
539	LSTM	SPINN	TD	539	0.236±0.026
539	LSTM	SPINN	GTD	All	0.325±0.037
539	CNN	Pure NN	N/A	539	0.283±0.069
539	CNN	Pure NN (General)	N/A	All	0.276±0.022
539	CNN	SPINN	HEC18	539	0.285±0.070
539	CNN	SPINN	TD	539	0.236±0.015
539	CNN	SPINN	GTD	All	0.250±0.022
742	LSTM	Pure NN	N/A	742	0.884±0.589
742	LSTM	Pure NN (General)	N/A	All	0.325±0.021
742	LSTM	SPINN	HEC18	742	0.388±0.036
742	LSTM	SPINN	TD	742	0.260±0.021
742	LSTM	SPINN	GTD	All	0.346±0.045
742	CNN	Pure NN	N/A	742	0.214±0.037

742	CNN	Pure NN (General)	N/A	All	0.310 ± 0.040
742	CNN	SPINN	HEC18	742	0.239 ± 0.055
742	CNN	SPINN	TD	742	0.233 ± 0.033
742	CNN	SPINN	GTD	All	0.335 ± 0.024

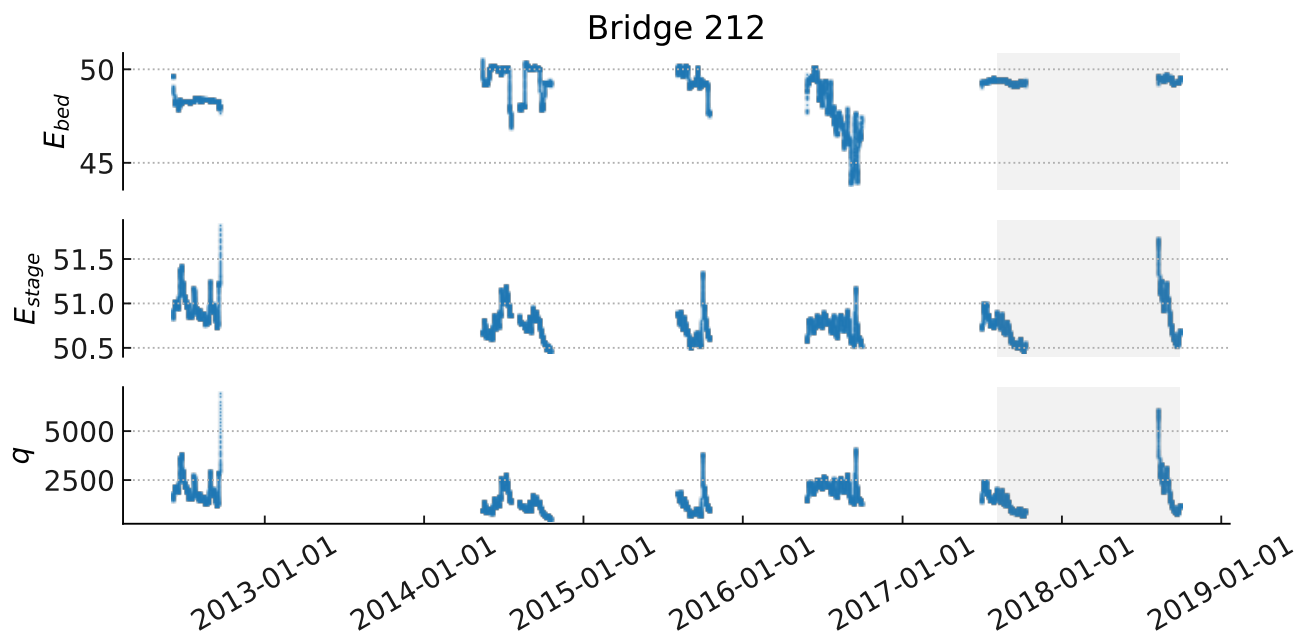


Fig. A1. Historical time series data for Bridge 212 shows the three features: bed elevation (m), river stage elevation (m), and discharge (m^3/s). The grey zone shows the test subset, and the transparent part before is the training and validation subsets.

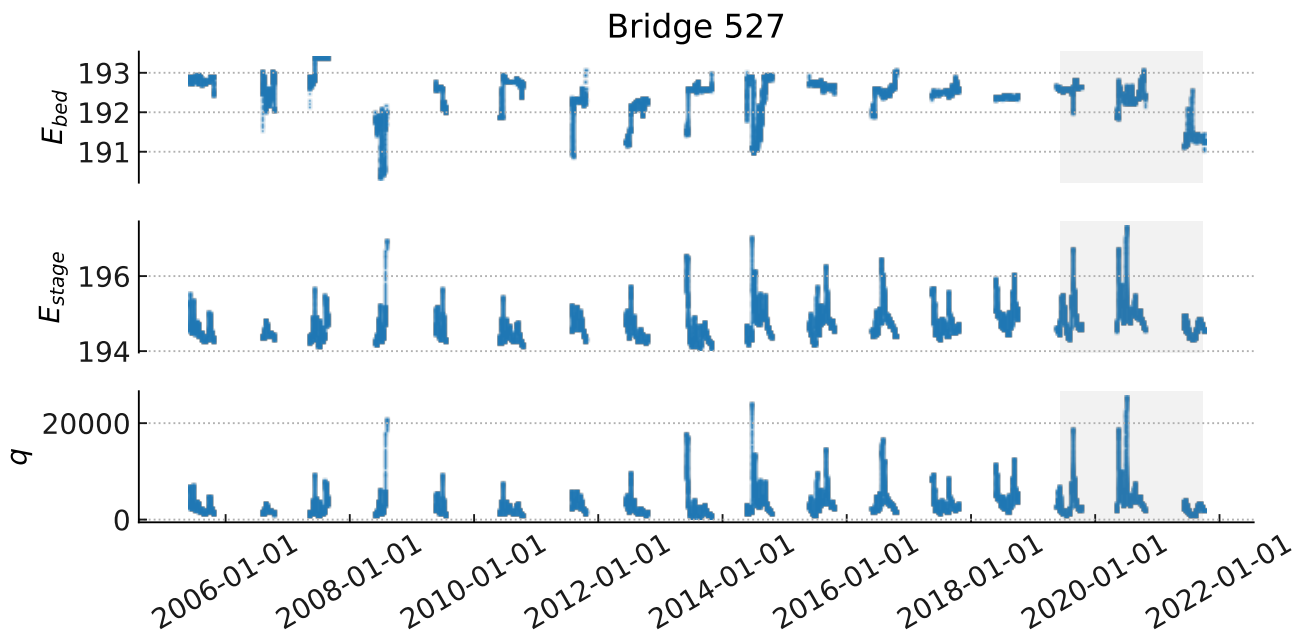


Fig. A2. Historical time series data for Bridge 527 shows the three features: bed elevation (m), river stage elevation (m), and discharge (m^3/s). The grey zone shows the test subset, and the transparent part before is the training and validation subsets.

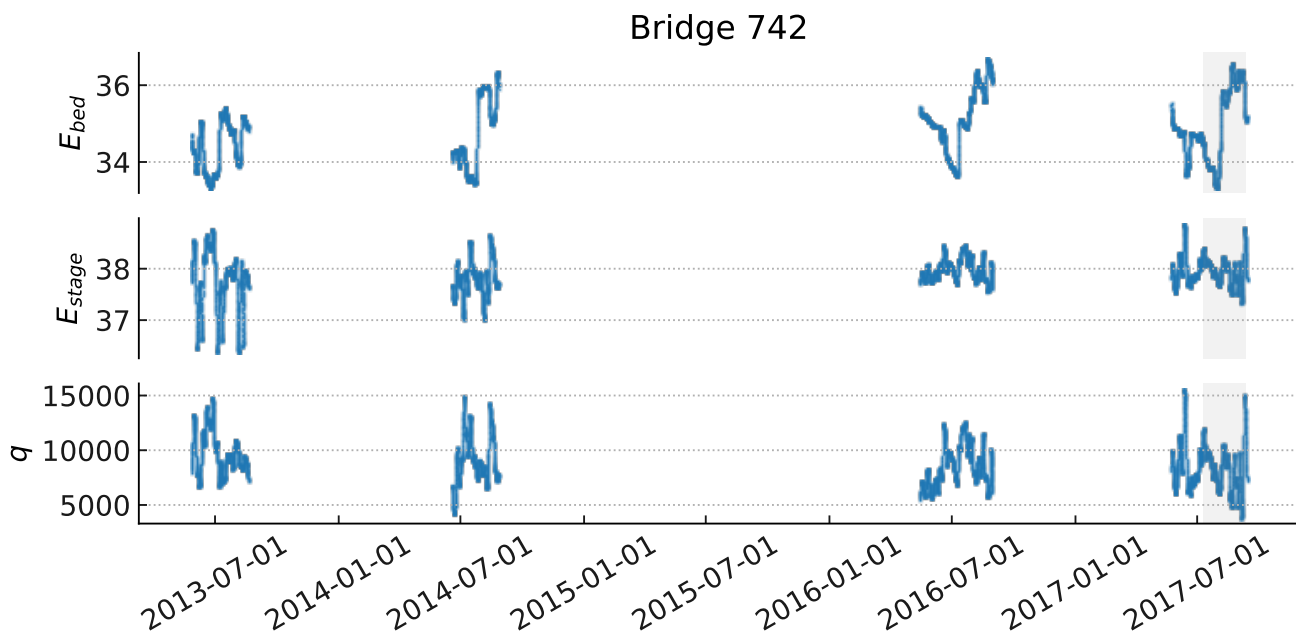


Fig. A3. Historical time series data for Bridge 742 shows the three features: bed elevation (m), river stage elevation (m), and discharge (m^3/s). The grey zone shows the test subset, and the transparent part before is the training and validation subsets.

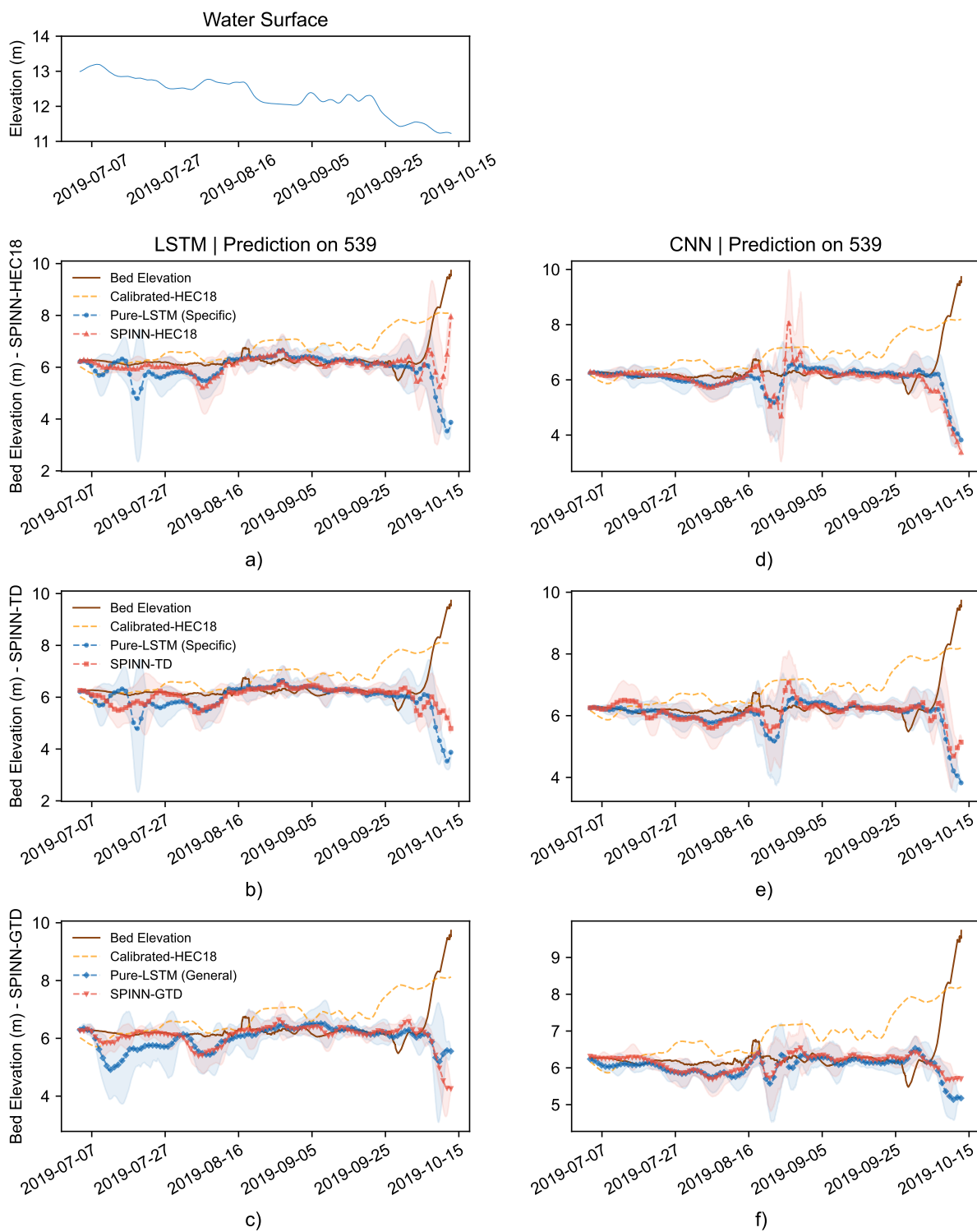


Fig. A4. Model predictions versus actual observations for Bridge 539 test set (July-October 2019). Top graph displays the flow changes in this period. (a-c) show LSTM-based predictions, (d-f) display CNN-based predictions, and each row represents SPINN-HEC18, SPINN-TD, and SPINN-GTD, respectively.

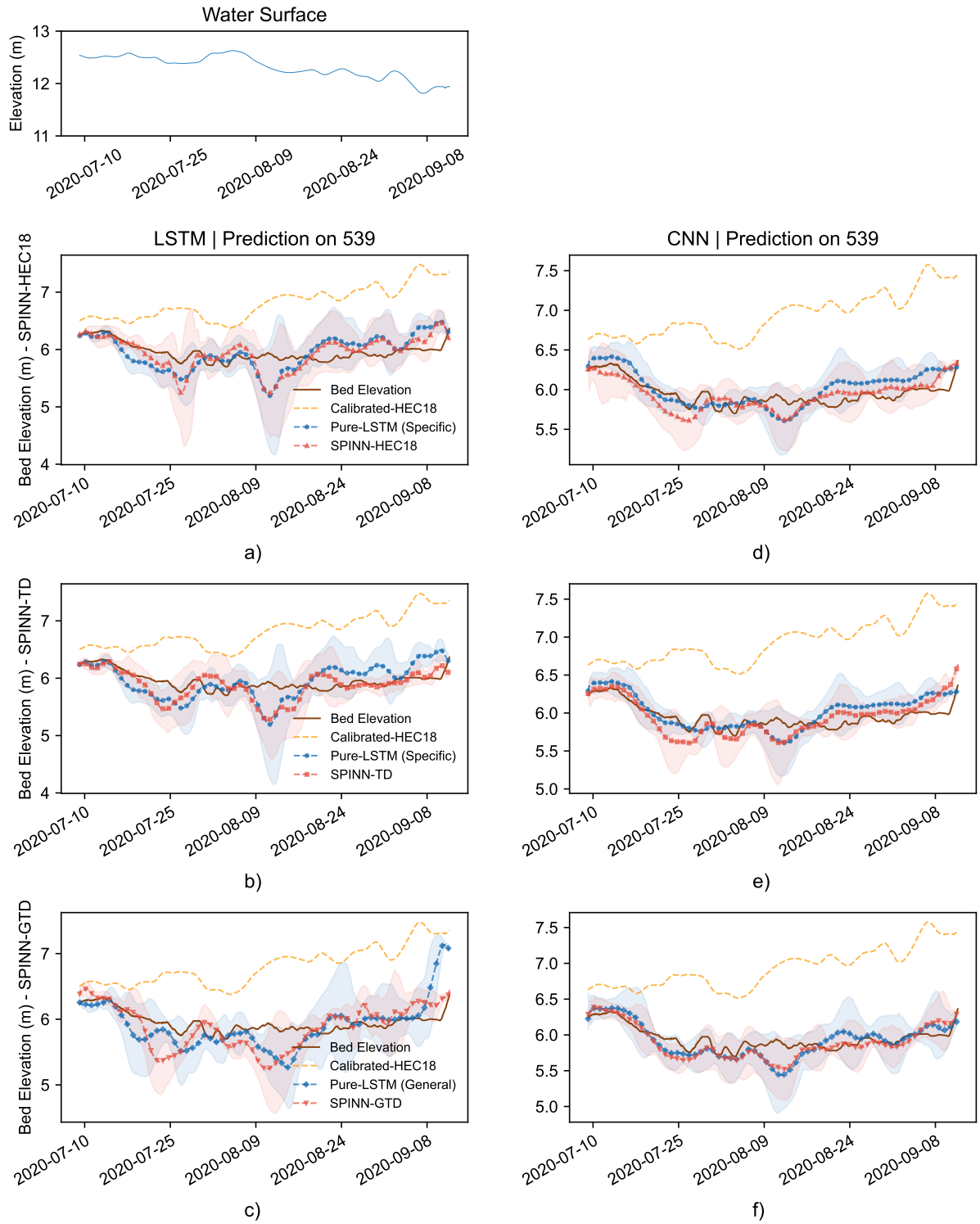


Fig. A5. Model predictions versus actual observations for Bridge 539 test set (July-September 2020). Top graph displays the flow changes in this period. (a-c) show LSTM-based predictions, (d-f) display CNN-based predictions, and each row represents SPINN-HEC18, SPINN-TD, and SPINN-GTD, respectively.